2012

Plasticization and reinforcement in a boron cage compound polyurethane nanocomposite: A dielectric study

J. Liu
Iowa State University

X. Zhang
Iowa State University

D. E. Bowen
National Nuclear Security Administration's Kansas City Plant

Nicola Bowler
Iowa State University, nbowler@iastate.edu

Plasticization and Reinforcement in a Boron Cage Compound Polyurethane Nanocomposite: A Dielectric Study

Authors: J. Liu[1], X. Zhang[1], D. E. Bowen[2], E. A. Eastwood[2], and N. Bowler[1]

Affiliations:

1: Department of Materials Science and Engineering, Iowa State University

2: Polymer Materials Engineering and Production, the National Nuclear Security Administration's Kansas City Plant, Operated by Honeywell Federal Manufacturing & Technologies, LLC

Abstract

In order to control and modify the physical properties of nanocomposite systems, it is essential to understand the nano-filler/polymer structure-property relationships. Boron cage compounds (BCCs) are a class of icosahedral, closed cage molecules that are of interest due to their high boron content and inherent neutron absorbing/shielding properties, and because of their ability to act as molecular nano-particles. When the BCC *n*-hexylcarborane is blended with a polybutadiene (PBD)/polyurethane (PU) segmented copolymer (EN8) an increase in the glass transition (T_g) temperature of the PBD phase (reinforcement) and a decrease in the T_g temperatures of the PU phases (plasticization) are observed. These observations were investigated by examining the dielectric relaxation properties of copolymer samples with and without added *n*-hexylcarborane (0wt% and 5wt% *n*-hexylcarborane) using broadband dielectric spectroscopy in the frequency range from 0.01 to 1 MHz and temperature range from -140 to 130 °C. Parametric fitting techniques aided in the identification of two α relaxation processes associated with the glass transitions of the soft PBD phase and the hard urethane phases, and a secondary β relaxation process due to the localized motions of side groups. The conductivities at low frequencies were also identified and modeled. Differential Scanning Calorimetry (DSC) did not indicate the presence of a crystalline component within the copolymer samples, so interfacial polarization (Maxwell-Wagner-Sillars) relaxation is not possible. A relaxation map (Arrhenius diagram) associated with these processes has been developed from the experimental data to elucidate the role of *n*-hexylcarborane in the molecular dynamics of the system. Values of fitting parameters, calculated T_g values, and a fragility index are also given for comparison. Reduced localized motion of the soft PBD phase, as well as reinforcement of the hard urethane phases is observed upon the introduction of *n*-hexylcarborane. The hypothesis that the *n*-hexylcarborane content preferentially locates within the hard urethane phases is supported by the observed decrease of the fragility index and T_g of the urethane phases.

Introduction

Segmented copolymers consist of $(AB)_n$ type alternating blocks. Their properties are affected by the intrinsic properties of the segments, including the chemical makeup of the segments, the polymerization method, the segment molecular weight and molecular weight distribution, the compatibility of the segments, the ability of the blocks to crystallize, and fabrication and processing methods. Segmented copolymers can range from random copolymers to thermoplastic elastomers. The former has been found in copolymers with short segment lengths

and similar inter- and intra-segment binding forces, and those compatible copolymers exhibit homogeneous morphology. Incompatible segmented copolymers are a class of thermoplastic elastomers that exhibit phase separation. The two-phase microstructure of $(AB)_n$ segmented copolymers arises from the thermodynamic incompatibility of the unlike blocks.

Segmented polyurethanes are a commercially important class of thermoplastics. These materials derive many of their useful properties from the incompatibility of the soft 'rubbery' and hard 'glassy' segments, and subsequent phase separation into separate domains. In the segmented urethane EN8, the soft phase primarily consists of low molecular weight polybutadiene (PBD) segments, which possess a T_g well below ambient temperature. The hard PU phases primarily consist of the aromatic diisocyanate portion of the polymer network and have glass transitions above the usage temperature. In EN8 and other polyurethanes, the hard 'glassy' phases act like cross-links at temperatures below the T_g of the PU phase. In general, these physical cross-links act to reinforce the polymer matrix and are responsible for increasing the thermal stability, stiffness, and Young's modulus of these materials at higher temperatures, and a variety of non-covalent interactions may participate (Figure 1) [1].

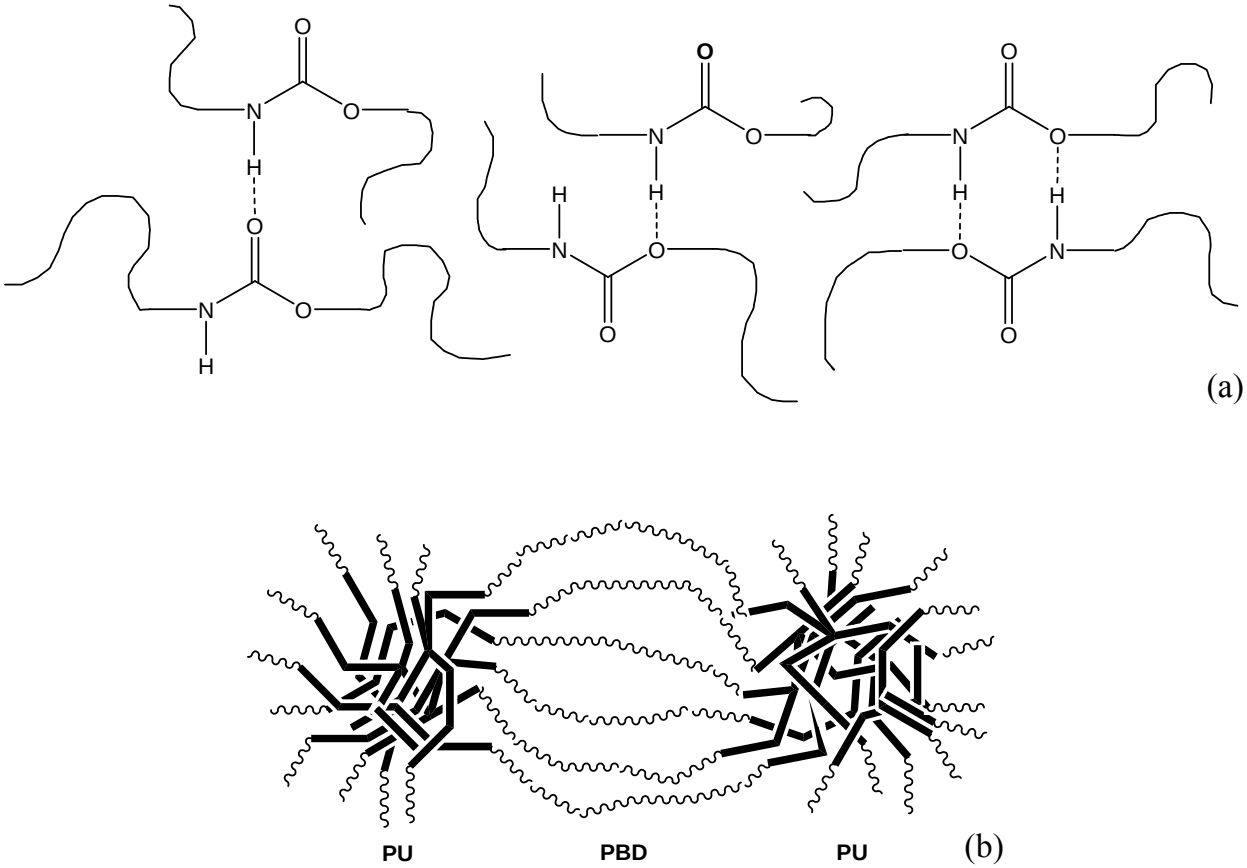

Figure 1. Possible crosslink structures of polyurethanes, which include hydrogen bonding (a) and phase separation of polyurethane (PU) and polybutadiene (PBD) phases (b).

The physical connection between the polymeric segments that comprise the phases produces an intimate relationship and interplay between them, with a change in one phase potentially

affecting a change in the other. Upon the introduction of the *n*-hexylcarborane, the soft, 'rubbery' PDB phase of EN8 is reinforced, while the hard, 'glassy' PU phase is plasticized. The mechanism causing the differing effects of *n*-hexylcarborane on the behavior of EN8 is of interest, because boron cage compounds are not widely considered to be molecular nano-particles and because reinforcement, in particular, is not expected. Although other analytical techniques such as, for example, electron microscopy, are appropriate for characterizing the phase morphology of segmented polyurethanes, broadband dielectric spectroscopy (BDS) has been shown to be effective in characterizing temperature- and frequency-dependent behavior. Since polar groups exist within both the soft and hard segments of EN8, BDS is a natural and effective tool for investigating the relaxation behaviors the associated phases, providing insight into their molecular dynamics and phase behavior.

Materials

EN8 Urethane

EN8 urethane was prepared by physically mixing 100 grams of EN4 (Part A, Figure 2) with 18.8 grams of EN8 (Part B, Figure 3). Of the 100 grams part A, 10 to 12 grams were free toluenediisocyanate (TDI) with the remaining 88 to 90 grams being a TDI-terminated polybutadiene (PBD) prepolymer. The diols of Part B (namely bis-(2-hydroxypropyl)aniline and 2-Ethyl-1,3-hexane diol) react with the TDI-terminated PBD prepolymer via the isocyanate groups to complete the chain extension. The excess TDI present also reacts with the diols of Part B.

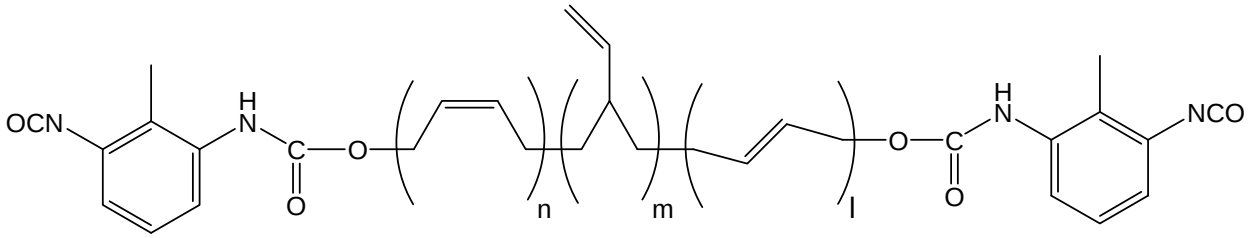

TDI End Capped PBD
Ratio n = 1.0; m = 1.0; l = 3.0
n + m + l = ~12

Figure 2. Part A - EN4 consists of 10 to 12 parts by weight of free toluenediisocyanate (TDI) and 88 to 90 parts by weight of TDI-terminated polybutadiene (PBD) prepolymer.

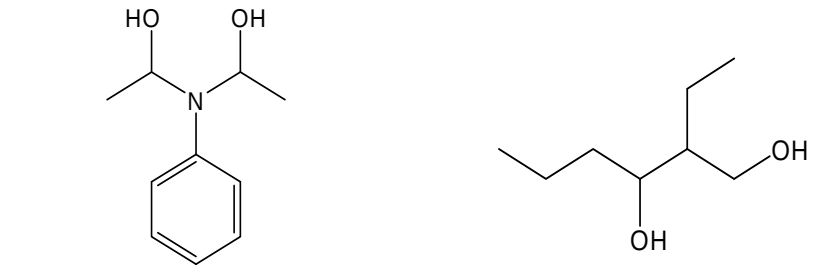

BHPA = Bis(2-Hydroxypropyl)aniline EHD = 2-Ethyl-1,3-Hexanediol

Figure 3. Part B - EN8 consists of bis-(2-hydroxypropyl) aniline and 2-ethyl-1,3-hexane diol.

Boron Cage Compounds

Boron cage compounds (BCCs) are a class of icosahedral, closed cage molecules (carboranes – *closo*-$C_2B_{10}H_{12}$, and dodecaborane anions or boranes –[*closo*-$B_{12}H_{12}$]-, Figure 4) that can be highly stable and non-toxic, and are easily modified chemically. They are of interest because of their high boron content and the inherent neutron absorbing/shielding properties they lend to polymer composites into which they have been incorporated. The ^{10}B isotope of boron, which is naturally abundant at ~20wt%, has a high cross-section for neutron capture.

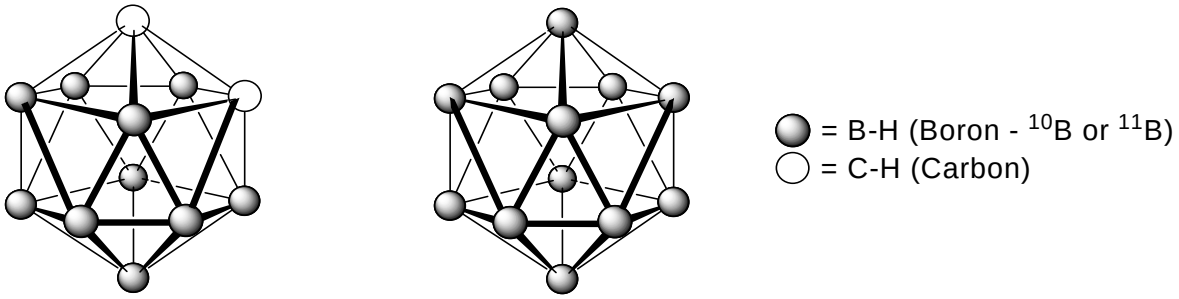

closo-1,2-$C_2B_{10}H_{12}$ Dodecaborane [*closo*-$B_{12}H_{12}$]$^{2-}$

Figure 4. Carboranes –*closo*-$C_2B_{10}H_{12}$, and dodecaborane anions or boranes –[*closo*-$B_{12}H_{12}$]$^-$.

Of particular interest is the BCC *n*-hexylcarborane; a highly soluble, low vapor pressure, high boiling temperature liquid (Figure 5). *n*-Hexylcarborane is also of interest because it does not easily sublime, unlike *closo*- $C_2B_{10}H_{12}$.

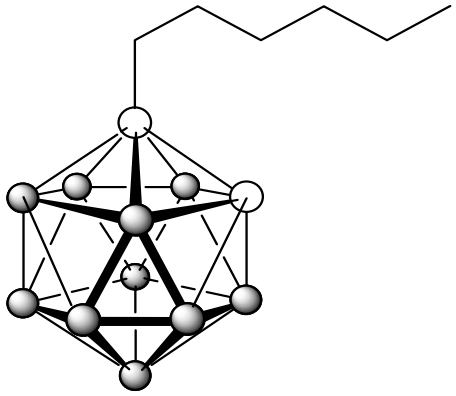

Figure 5. The BCC n-hexylcarborane.

Sample preparation

EN8 urethane filled with *n*-hexylcarborane was prepared by adding *n*-hexylcarborane to Part A, EN4 described above, and physically mixing with Part B. Films approximately 1.5 mm thick, containing 0 and 5% by weight of *n*-hexylcarborane were prepared by degassing for 5 min and then pressing at 110 ˚C for 30 min. The resulting samples appear clear and pale tan colored. Circular samples with diameters of approximately 20.8 mm, suitable for dielectric spectroscopy, were punched from the films. The thickness and standard deviation of the samples was measured at six different points on the sample, and the mean and standard deviation of these measurements are listed (Table 1).

Table 1. Thickness of EN8/*n*-hexylcarborane samples. 'EN8/0*n*-hex' refers to an EN8 sample to which no *n*-hexylcarborane has been added. 'EN8/5*n*-hex' refers to an EN8 sample to which 5wt% *n*-hexylcarborane has been added.

Sample	Thickness (mm)
EN8/0*n*-hex	1.575 ± 0.005
EN8/5*n*-hex	1.573 ± 0.008

Experiment

Rheology

The glass transition temperatures of the samples were first determined rheologically. Rheology testing was performed on a TA Aries 2000 or AR-G2 rheometer under torsion between 25 mm parallel plates. Disks with diameter ~11 mm and thickness ~3.52 mm were used as samples. To the extent possible, the samples were of uniform size. Samples that were initially thicker than ~3.52 mm were sanded with an ultra-fine grit sand paper. Although care was taken to ensure

uniform thickness within a sample and from sample to sample, and sample thickness was measured using calibrated calipers, some slight thickness variation was observed. All samples were subjected to a temperature sweep from low to high temperatures at strains varying from 0.1 % to 0.025 % at a frequency of 1 Hz. All experiments where performed under normal force control at 5.0 N with a 0.5 N tolerance, maintained provided that the sample thickness remains within ± 500 μm of its initial value. The temperature range explored for each sample was selected depending on the values of the expected transition temperatures. A 10 to 20 minute equilibration time was used once a sample reached the minimum (starting) temperature. Thereafter, a temperature ramp rate of 3 ˚C/min was used.

Differential Scanning Calorimetry

Differential scanning calorimetry (DSC) is a thermal analysis technique in which the difference in the amount of heat required to increase the temperature of the sample under test and to increase that of a reference sample is measured as a function of temperature. Here, DSC is conducted to establish the degree of crystallinity of the samples. Melting of a crystalline phase is observed as an endothermic peak in the DSC test. EN8/0*n*-hex and EN8/5*n*-hex samples were tested over the temperature range from 30 to 270 °C with a heating/cooling rate of 20 °C/min.

Dielectric Spectroscopy

The complex permittivity of the samples was measured, using a Novocontrol dielectric spectrometer, with automatic temperature control from -140 to 130 °C with a 5 °C temperature increment over a frequency range from 0.01 Hz to 1 MHz. Electrodes with 20 mm diameter were used.

Results

Rheology

The positions of the peak maxima in the loss tangent (tan δ) show that the PBD segments are reinforced slightly by the introduction of *n*-hexylcarborane into EN8 urethane. The tan δ peak maximum is a measure of a polymeric glass transition temperature. On the other hand, the PU segments are plasticized by the presence of the molecular nano-filler (Chart 1). As determined by rheology, the T_g of the PBD segment of EN8/0*n*-hex is around -75ºC and those of the two broad PU segment transitions are observed at around 49 ºC and 72 ºC. With the introduction of *n*-hexylcarborane into EN8, the T_g of the urethane component is observed to decrease by approximately 8 ºC, while T_g of the PBD segment increases slightly by a maximum < 5 ºC, over the range of 0-5wt% added *n*-hexylcarborane. These results are summarized (Table 2).

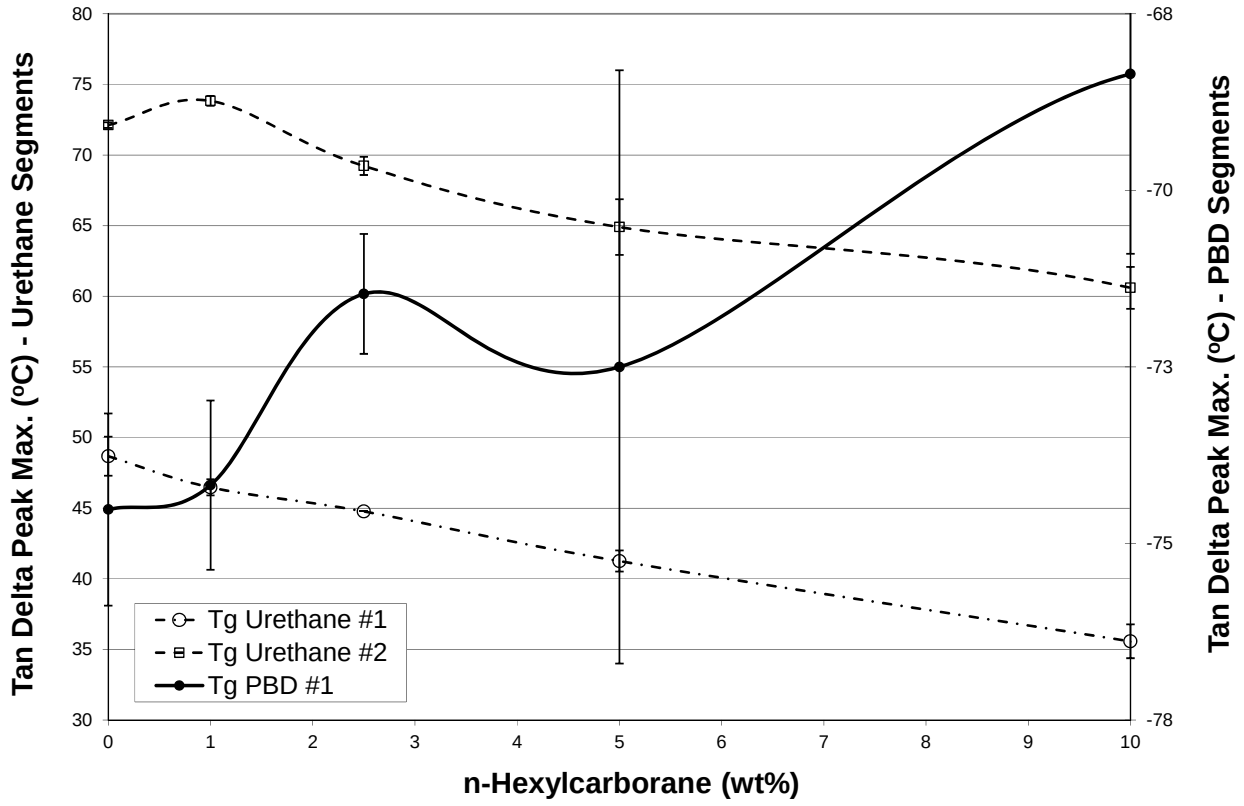

Figure 6. The changes in the loss tangent peak maxima (T_g) of the PU Segment #1, PU Segment #2, and PBD segment transitions as a function of increasing *n*-hexylcarborane wt%.

Table 2. Rheologically determined transition temperatures of EN8/0*n*-hex and EN8/5*n*-hex.

Segment, sample	$\sim T_g$ (ºC)
PU Segment #1, EN8/0*n*-hex	72
PU Segment #1, EN8/5*n*-hex	65
PU Segment #2, EN8/0*n*-hex	49
PU Segment #2, EN8/5*n*-hex	41
PBD, EN8/0*n*-hex	-75
PBD, EN8/5*n*-hex	-72

Differential Scanning Calorimetry

The results of initial DSC testing on EN8/0*n*-hex (Figure 7) and EN8/5*n*-hex (Figure 8) are shown below. Exothermic peaks are observed between 175 ºC and 185 ºC. The observed exotherms can be attributed to additional curing taking place in the samples between unreacted starting materials remaining after processing. The endothermic peaks observed at approximately 60 °C can be attributed to the melting of the crystalline diol units in the samples. The exothermic peaks observed between 175 and 185 °C occur in the same temperature range in which an endothermic peak is expected if there is crystallinity in the PU segments. It is not possible, therefore, to determine from these initial DSC tests whether or not crystallinity exists within the sample. To resolve the question of whether or not crystallinity exists in the samples, subsequent DSC testing was performed by cooling the sample following the initial DSC test. Under these conditions, the presence of crystallinity would be indicated by exothermic peaks visible on cooling, indicating the formation of the crystalline phase. It was found, however, that the DSC cooling curves are featureless, indicating that no crystallization process occurs during cooling and that EN8/0*n*-hex and EN8/5*n*-hex are amorphous.

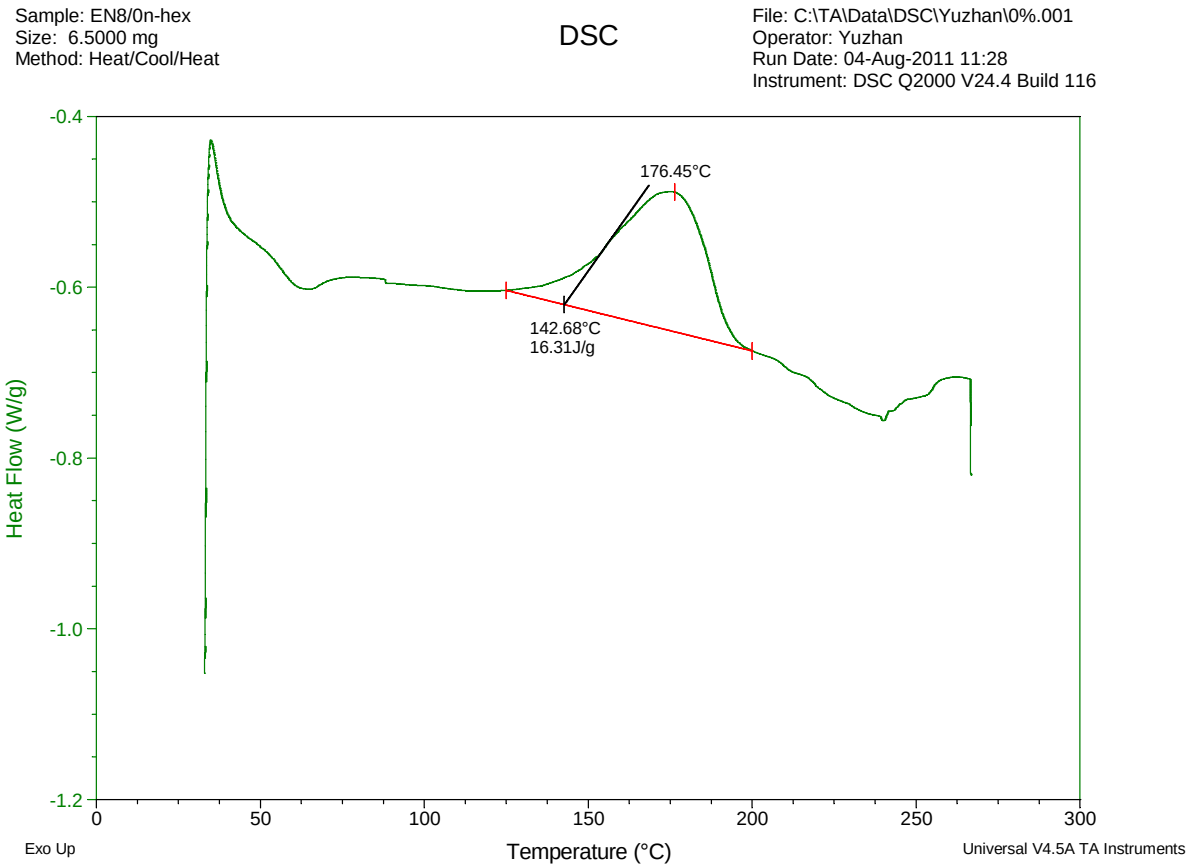

Figure 7. Heat flow measured as sample EN8/0*n*-hex is heated at 20 °C/min.

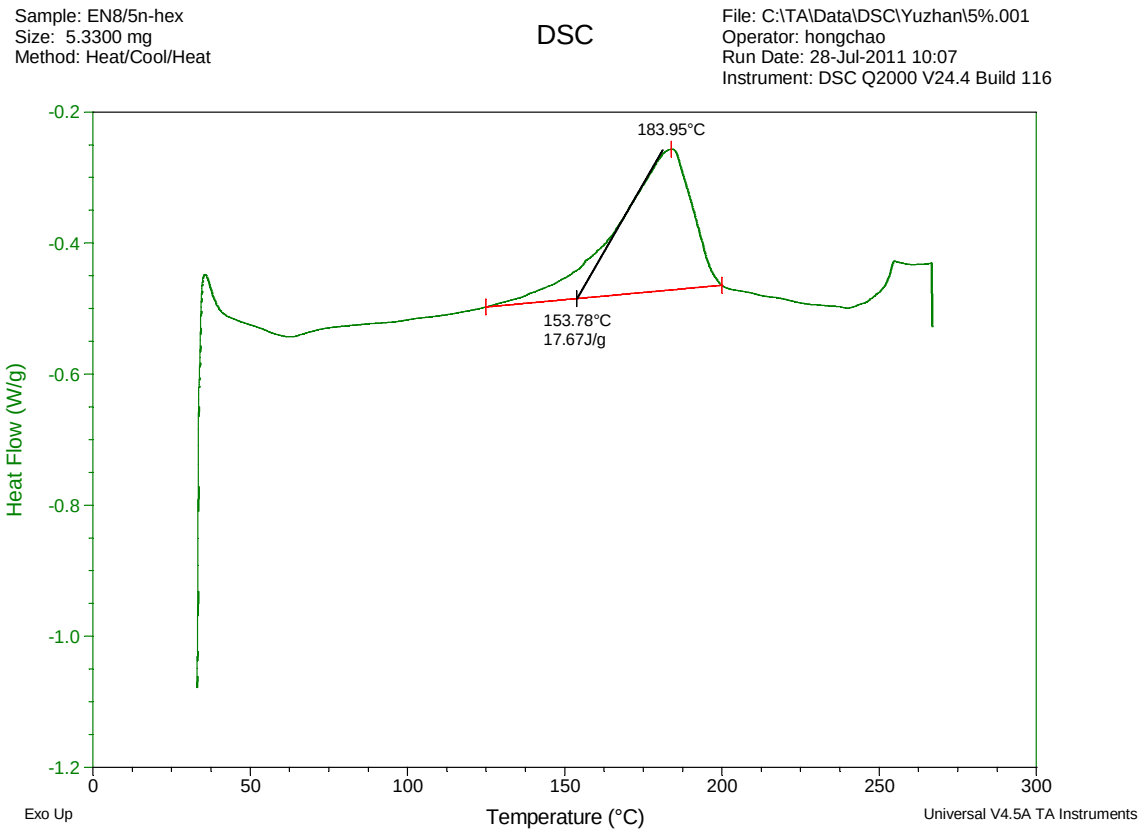

Figure 8. Heat flow measured as sample EN8/5*n*-hex is heated at 20 °C/min.

Dielectric Spectroscopy

Plots of the imaginary permittivity of the EN8/0*n*-hex (Figure 9) and EN8/5*n*-hex (Figure 10) samples, measured as a function of frequency and temperature, exhibit two distinct transitions. Data extracted from the imaginary permittivity plots, namely the real and imaginary parts of the permittivity of the EN8/0*n*-hex (Figure 11) and EN8/5*n*-hex (Figure 12) samples, more precisely show these transitions as a function of temperature and frequency. Due to the fact that the T_g for EN8 occur from approximately -85°C to -40°C for the soft segment and -20°C to 105°C for the hard segment, it is reasonable to assign the peaks of the imaginary part of permittivity at lower temperature as the α relaxation of the PBD phase and the peaks at higher temperature as the α relaxation of PU phase. Modeling of the dielectric spectra allows the characteristics of individual relaxations to be extracted, enabling the effect of the *n*-hexylcarborane to be better understood. In particular, it allows the effect of the presence of PBD and PU segmental and polar side group motions to be elucidated.

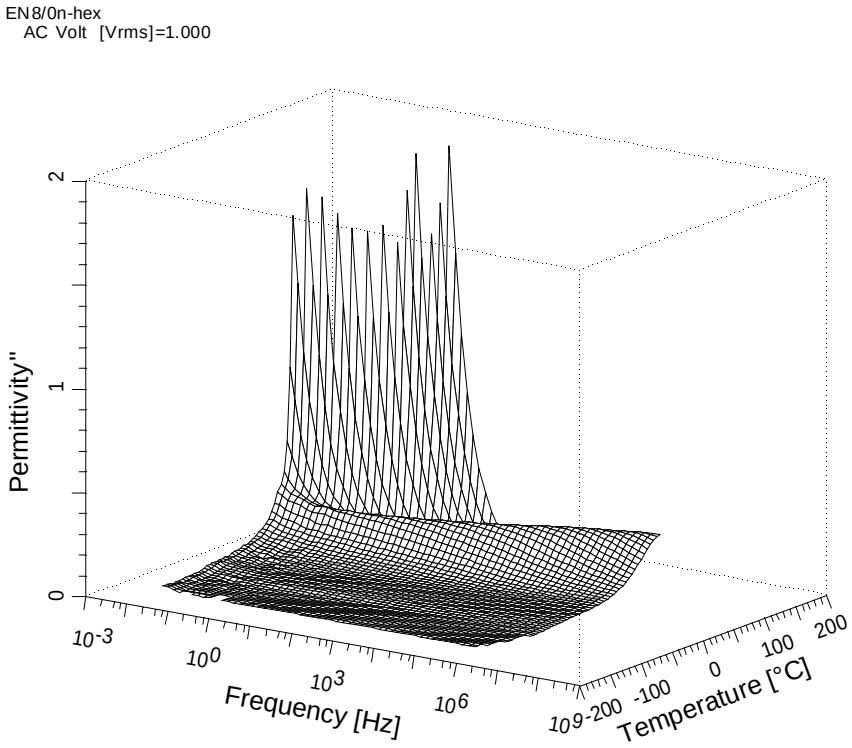

Figure 9. Imaginary permittivity of EN8/0*n*-hex as a function of frequency and temperature.

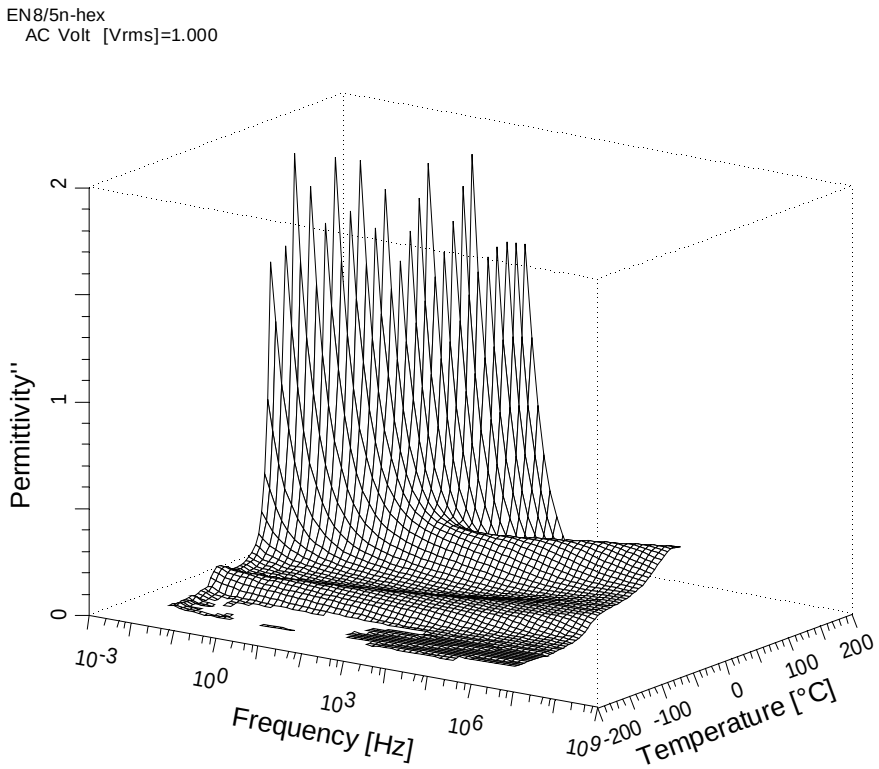

Figure 10. Imaginary permittivity of EN8/5*n*-hex as a function of frequency and temperature.

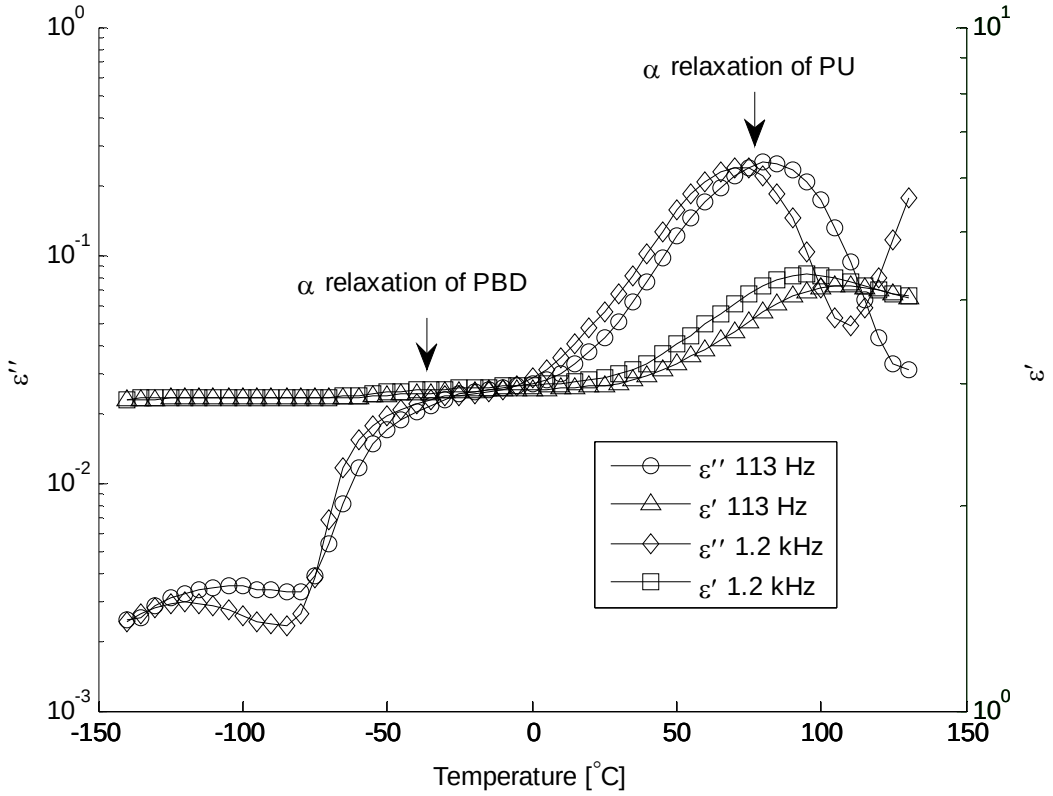

Figure 11. Real and imaginary permittivity of EN8/0*n*-hex as a function of temperature at 113 Hz and 1.20 kHz.

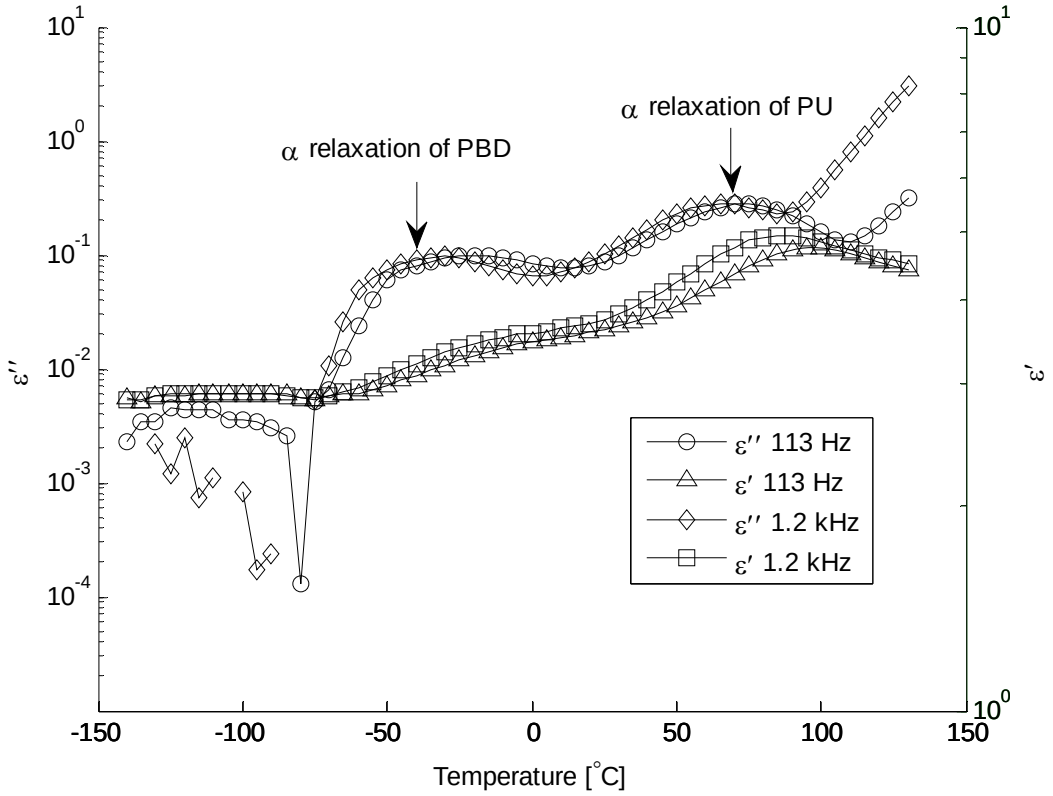

Figure 12. Real and imaginary permittivity of EN8/5*n*-hex as a function of temperature at 113 Hz and 1.20 kHz.

Modeling the Dielectric Spectrum

In order to extract more precise information about the observed relaxations and their associated molecular dynamics, the α-type glass transitions, a secondary β-type relaxation process, and a conductivity term in the dielectric spectrum are modeled by the parametric Havriliak-Negami approach [2]. The dielectric spectrum is decomposed as the sum of four relaxations and a conductivity term, as described by Equation (1), and the best fit between experimental data and the model is obtained by least squares regression [3, 4].

$$\varepsilon^*(\omega) - \varepsilon_\infty = \sum_{p=1}^{4} \frac{\Delta\varepsilon_p}{[1 + (i\omega\tau_{p,HN})^{1-\alpha_{p,HN}}]^{\beta_{p,HN}}} - \frac{i\sigma}{\varepsilon_0\omega^A} \qquad (1)$$

In (1), ω is angular frequency, p = 1,…, 4 denotes the different relaxation types, $\Delta\varepsilon$ is the dielectric strength, ε_∞ is the permittivity well above the frequency of the measurement, σ is the conductivity, ε_0 is the permittivity of free space, and τ_{HN}, α_{HN} and β_{HN} are characteristic

relaxation time and shape parameters that describe the Havriliak-Negami function [2]. The term containing the power A is due to conductivity and electrode effects. A is always smaller than 1. It is common to proceed by fitting the imaginary part of the permittivity, $\varepsilon''(\omega)$. By using the least squares fitting techniques, the fitting parameters then satisfy the following criterion:

$$\sum_i \left[\left(\varepsilon''_{exp}\right)_i + \frac{\sigma_{DC}}{\varepsilon_0 \omega_i^A} - \sum_{p=1}^{2} \varepsilon''_{p,HN}(\omega_i) \right]^2 \rightarrow \min \qquad (2)$$

where the sum is over the i experimental data points and

$$\varepsilon''_{p,HN}(\omega_i) = \mathrm{Im}\left\{ \frac{\Delta\varepsilon_p}{\left[1 + \left(i\omega\tau_{p,HN}\right)^{1-\alpha_{p,HN}}\right]^{\beta_{p,HN}}} \right\}.$$

Above the T_g, the glassy state is transformed to a rubbery state. The segmental motions and chain connectivity of polymers both contribute to the dynamic glass transition by intramolecular and intermolecular cooperativity. The characteristic relaxation rate of the α relaxation, which describes the viscosity and structural relaxation, obeys the Vogel-Fucher-Tammann (VFT) law [5-7]

$$f_{\max}^{\alpha} = f_0 \exp\left(-\frac{DT_0}{T - T_0}\right) \qquad (3)$$

in which D is the strength parameter and the temperature T_0 is characteristic of static dipolar freezing of dipolar motion in the absence of long-range correlation.

The fragility of polymers, with index m [8], is related to the curvature in the plot of $\log_{10}(f_{max})$ versus 1/T, and is given by

$$m = \frac{d\log_{10}\left(\frac{1}{2\pi f_{max}}\right)}{dT/T_0}\Big|_{T=T_g}. \qquad (4)$$

The fragility index m of the sample can be described by the following formula [5] in terms of VFT parameters,

$$m = \frac{T_g}{\ln(10)} \frac{DT_0}{(T_g - T_0)^2} \qquad (5)$$

The dielectric β relaxation process of amorphous polymers arises from localized rotational fluctuations of side chains. The mechanisms of the β relaxation were discussed by Goldstein and Johari [9, 10] who argued that the β relaxation universally exists in a great variety of amorphous polymers. The temperature dependence of the characteristic relaxation time of the β relaxation follows the Arrhenius law,

$$f_{\max}^{\beta} = f_0 \exp\left(-\frac{E_A}{k_B T}\right) \qquad (6)$$

where the factor f_0 is on the order of the vibrational frequency of the localized motions, E_A is the activation energy of the β relaxation, and k_B is the Boltzmann constant.

The relation between maximum relaxation time and the corresponding Havriliak-Negami parameters α_{HN} and β_{HN} in Equation (1) are [8]

$$f_{max}^{\alpha,\beta} = f_{HN}^{\alpha,\beta} \left\{ \frac{\sin\left[\frac{\pi(1-\alpha_{HN})\beta_{HN}}{2(\beta_{HN}+1)}\right]}{\sin\left[\frac{\pi(1-\alpha_{HN})}{2(\beta_{HN}+1)}\right]} \right\}^{-1/(1-\alpha)} , \qquad (7)$$

where $f_{HN}^{\alpha,\beta} = 1/(2\pi\tau_{HN}^{\alpha,\beta})$ is the characteristic frequency of the α and β relaxations.

To show an example of the fit of the model to the data, isothermal plots, at 60 °C, of imaginary relative permittivity are shown for EN8/0*n*-hex (Figure 13) and EN8/5*n*-hex (Figure 14) samples, in which α and β relaxation processes and a conductivity terms are identified. The superposed relaxations and conductivity term agree well with the experimental data, where the standard errors of modeling results are 0.0016 and 0.526 for EN8/0*n*-hex and EN8/5*n*-hex, respectively. Isothermal data sets were modeled at other temperatures with similar standard errors. The Arrhenius diagram of the α and β relaxation processes of the investigated samples is plotted (Figure 15).

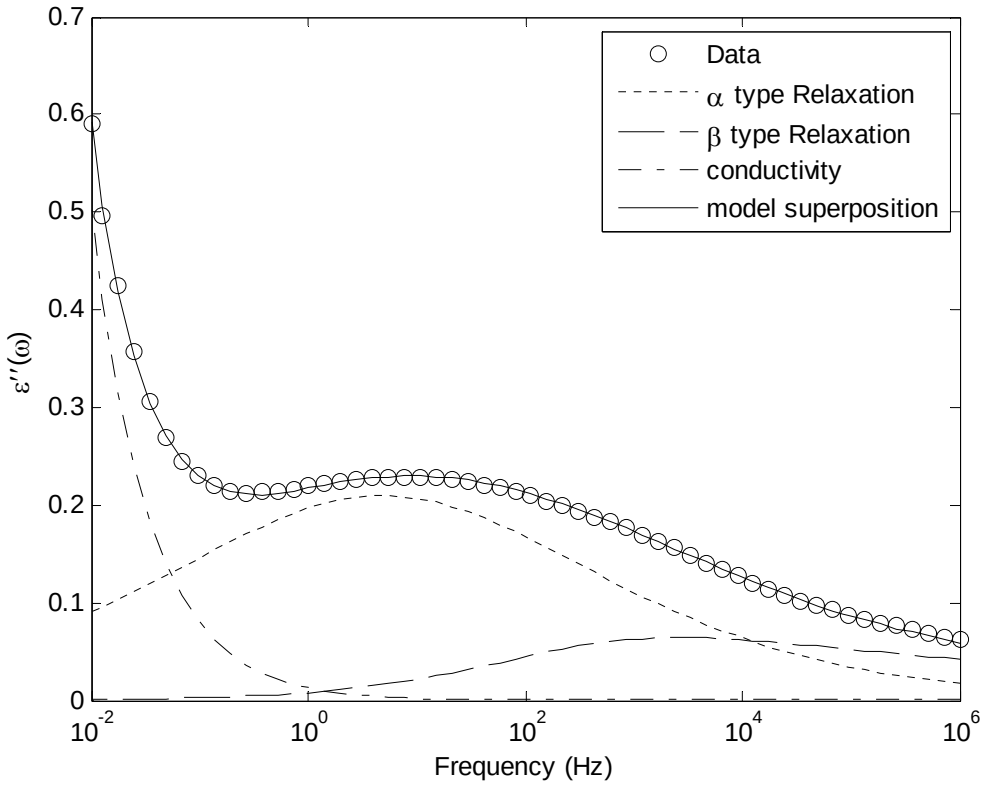

Figure 13. Imaginary relative permittivity, ε_r'', of EN8/0*n*-hex at 60 °C, plotted as a function of frequency.

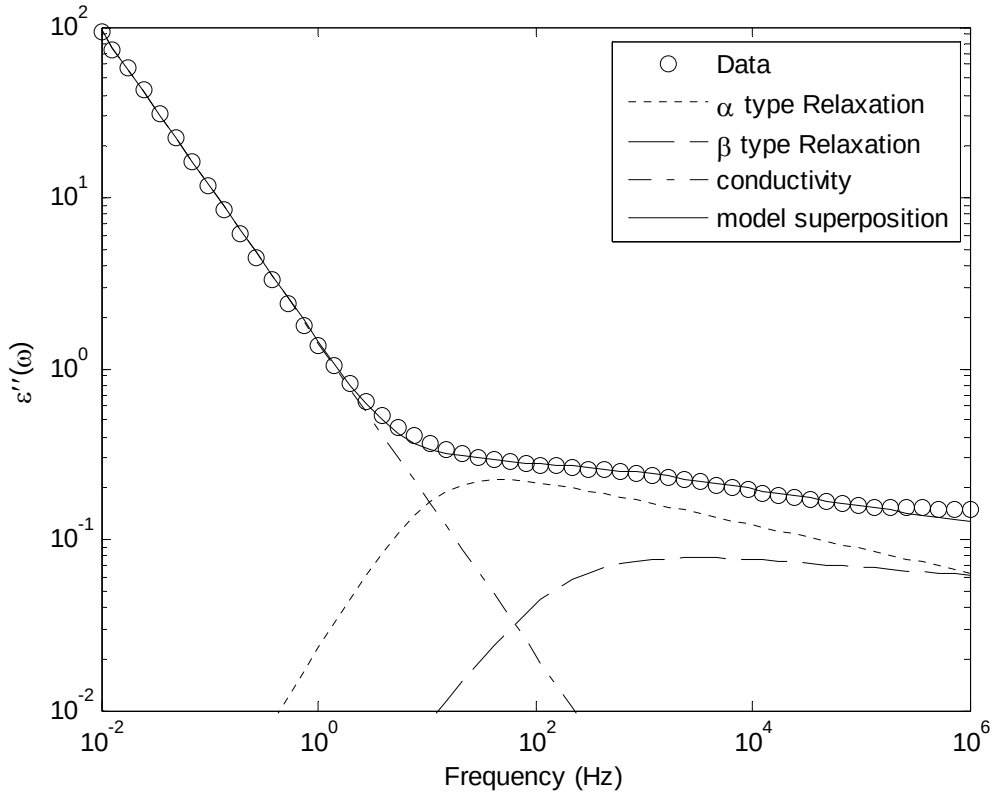

Figure 14. Imaginary relative permittivity, ε_r'', of EN8/5*n*-hex at 60 °C, plotted as a function of frequency.

The frequency-dependent imaginary permittivity data was modeled in this way at all temperatures from -140 to 130 °C at 5 °C temperature increments. The relaxation behavior of the two samples is compared in the Arrhenius plot (Figure 15), which shows the α and β relaxations of the PBD and PU segments in EN8/0*n*-hex and EN8/5*n*-hex. The fitted parameters of the α and β relaxations according to Equations (3) to (6) are listed in Table 3 and Table 4.

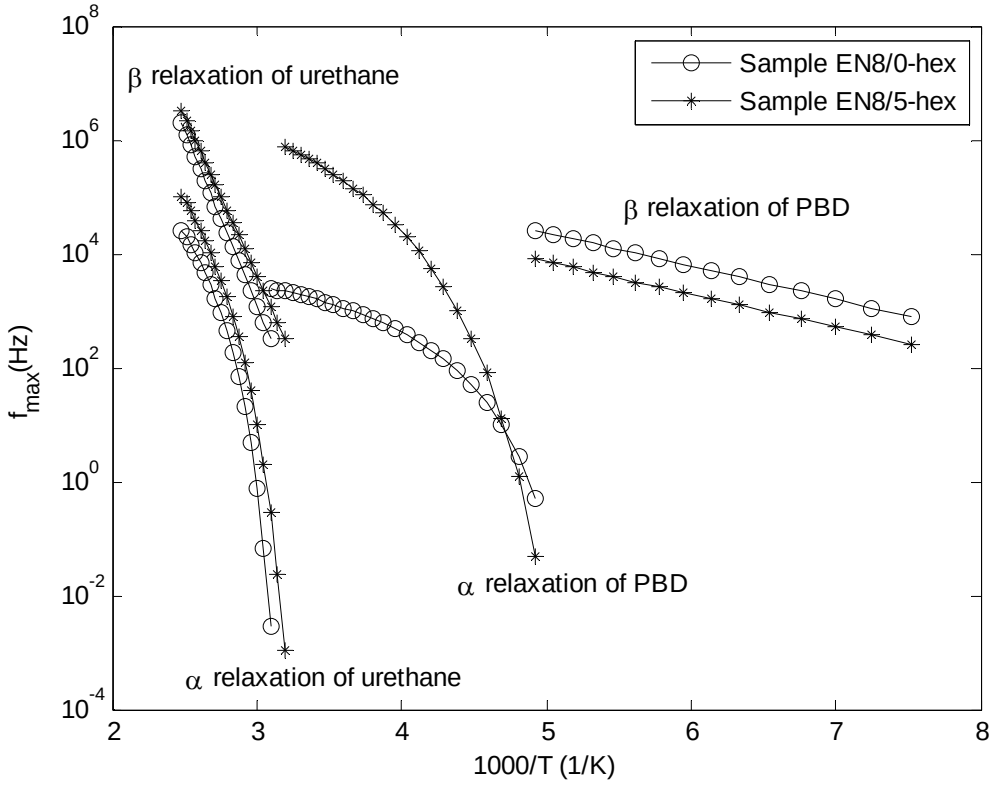

Figure 15. Arrhenius diagram for EN8/0*n*-hex and EN8/5*n*-hex, where f_{max} is the characteristic frequency of the maxima that appear in the isothermal plots of $\varepsilon''(\omega)$. The lines plotted in this figure are obtained by polynomial fits to the data points and serve only as a guide to the eye.

Table 3. Fitted parameters of the temperature dependence of the α relaxation processes of EN8/0*n*-hex and EN8/5*n*-hex, according to Equations (3) to (5).

Segment, sample	f_0 (Hz)	D	T_0 (ºC)	T_g (ºC)	m
Urethane, EN8/0n-hex	9.15×10^{6}	2.17	293.8	49.3	111 ± 6
Urethane, EN8/5n-hex	1.74×10^{8}	3.39	276.7	40.6	94 ± 5
PBD, EN8/0n-hex	1.43×10^{4}	1.42	178.3	-78.9	85 ± 4
PBD, EN8/5n-hex	4.36×10^{7}	3.14	176.1	-73.8	90 ± 5

Table 4. Fitted parameters of the temperature dependence of the β relaxation processes of EN8/0*n*-hex and EN8/5*n*-hex, according to Equation (6).

Segment, sample	A	E_A (kJ)
Urethane, EN8/0n-hex	4.19×10^{21}	118 ± 6
Urethane, EN8/5n-hex	2.63×10^{20}	107 ± 5
PBD, EN8/0n-hex	2.03×10^{7}	11.0 ± 0.6
PBD, EN8/5n-hex	5.49×10^{6}	11.0 ± 0.6

Discussion

The molecular dynamics of EN8 change significantly when *n*-hexylcarborane is introduced. As shown in Table 2 and Table 3, in which T_g values obtained by rheology and dielectric spectroscopy are in good agreement, the T_g of the PBD phase increases with the introduction of *n*-hexylcarborane, while that of the urethane phases decreases. In other words, both plasticization and reinforcement of EN8 occur upon the addition of *n*-hexylcarborane. Of particular interest is the observed increase in the T_g of the PDB phase of EN8/*n*-hexylcarborane, because polybutadiene alone is known to be highly plasticized by *n*-hexylcarborane, as observed by a significant decrease in loss tangent (tan δ) peak maximum.

The absence of any crystalline phase in the samples, as indicated by DSC experiments (Figures 7 and 8) suggests that the observed relaxation mechanisms do not include interfacial polarization (also known as Maxwell-Wagner-Sillars) relaxation. Further, since in general the glass transitions for EN8 occur from approximately -85 °C to -40 °C for the soft segment and -20 °C to 105 °C for the hard segment [11], the observed α relaxations can be assigned accordingly, and other observed relaxations are attributed to localized motions of sidegroups in the form of β relaxations.

One possible mechanism of reinforcement of the PBD segments in EN8/*n*-hexylcarborane is that the PU phase is preferentially *n*-hexylcarborane soluble causing it to swell. Preferential swelling of the PU phase might then cause a concomitant stretching of the less soluble PBD polymer segments within the PBD phase (Figure 16) resulting in restricted motion of the PBD polymer segments, accounting for the observed increase in the T_g of the PBD phase. This hypothesis does not require that the PBD phase be insoluble or even partially soluble in *n*-hexylcarborane, only less soluble than the PU phase. Although other mechanisms may be in effect, including increased inter-phase solubility with increasing *n*-hexylcarborane, we look to the results of this research for evidence supporting or refuting the hypothesis.

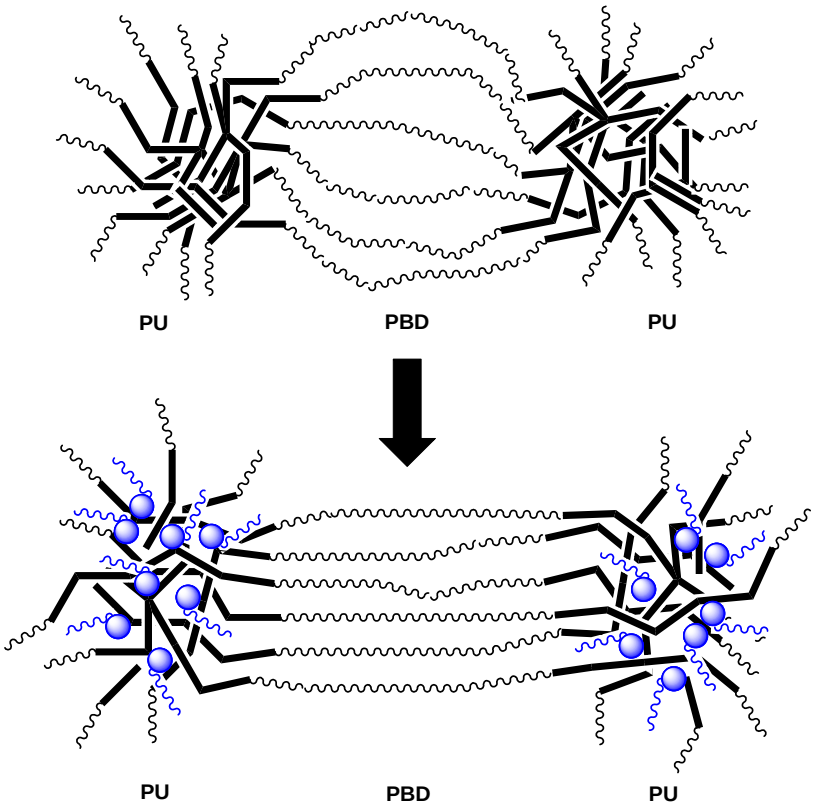

Figure 16. Schematic diagram showing hypothesized mechanism of reinforcement in EN8 urethane/*n*-hexylcarborane in which the hard PU component of EN8 swells, stretching the PBD polymer segments and causing the observed increase in T_g of the PBD phase.

With respect to the mechanism of reinforcement within the PDB phase of EN8/*n*-hexylcarborane composites, there are a number of considerations. These include the fitted parameters of the temperature dependence of the α-relaxation processes of the samples (Table 3), the reduction in T_g of the PU phase upon the introduction of *n*-hexylcarborane into EN8 and the associated reduction in the fragility index m, and the observed increase in T_g of the PBD phase and accompanying increase in m for PBD. Typically, in a composite, the fragility depends on the particle-polymer interactions and m is expected to increase or decrease due to attractive or repulsive particle-polymer interactions, respectively. The reduction in m for PU therefore indicates the presence of repulsive particle-polymer interactions for the PU segment and, conversely, the increase in m for PBD indicates the presence of attractive particle-polymer interactions. In reference [12], the authors report on the primary association of TiO_2 nanoparticles with N-H groups in PU hard segments leading to an increase in the extent of soft domains with high segmental mobility. In that case, lower T_g and m were observed. The observation here, that Tg and m of the PU segments are reduced upon the introduction of *n*-hexylcarborane into EN8, may be explained by the same attraction between the nanoparticles, here *n*-hexylcarborane, and N-H or other groups in PU. This is consistent with the hypothesis that the PU phase of EN8 is preferentially soluble in *n*-hexylcarborane.

Also of consideration are the β relaxations of the PBD phase of the two samples (Figure 16). It can be seen that the β relaxation frequency of the PBD phase of EN8/0*n*-hex is higher than that of EN8/5*n*-hex. This means that the localized motion of dipolar polyether side groups in the PBD segments of EN8/0*n*-hex is faster than that of the EN8/5*n*-hex sample. Conversely, in the hard PU segments, the β relaxation frequency of the PU segment of EN8/5*n*-hex is higher than that of EN8/0*n*-hex. This means that the localized motion of ester complexes [13] in the PU segments of EN8/5*n*-hex is faster than those of the EN8/0n-hex sample. Together, these observations indicate that the introduction of *n*-hexylcarborane into EN8 produces greater freedom of motion of the localized alkyl side groups in PU, but restricts the motion of the polyether side groups in PBD. This result is consistent with the hypothesis, knowing that an external mechanism of reinforcement is necessary to explain the observed increase in T_g and that *n*-hexylcarborane plasticizes polybutadiene alone.

Conclusion

The dielectric spectrum of EN8 segmented polyurethanes with 0 and 5% *n*-hexylcarborane by weight are investigated by broadband dielectric spectroscopy and parametric modeling. Upon introduction of *n*-hexylcarborane into EN8, reduced localized motion and reinforcement of the soft PBD phase, and plasticization of the hard urethane phase, are inferred by analysis of the T_g and fragility index; parameters obtained by modeling the dielectric spectrum. The observed results of this research are consistent with the hypothesis that the PU phase of EN8 is preferentially solubilized by *n*-hexylcarborane, possibly due to favorable interactions with N-H and other groups within polymer segments making up that phase. This, in turn, causes the hard PU phase of EN8 to swell, which in turn decreases its fragility index and T_g. Preferential swelling of the PU phase then causes the polymer segments of the less soluble PDB phase to stretch, resulting in restricted motion and an observed increase in the T_g of the PBD phase.

US Patent Number 8,193,292 , Polymers Containing Borane or Carborane Cage Compounds and Related Applications, Issued 6/5/12
US Patent Application Number, 12/816,555, Compositions Containing Borane or Carborane Cage Compounds and Related Applications, Filed 6/16/10

References

[1] B. Bengtson, C. Feger, W. J. Macknight, N. S. Schneider, Polymer, vol. 6, pp. 895-900, 1985.
[2] S. Havriliak, S. Negami, Polymer, vol. 8, pp. 161, 1967.

[3] E. Schlosser and A. Schonhals, Colloid Polym.Sci., vol. 267, pp. 963, 1989.
[4] J. Turnhout, M. Wubbenhorst, Dielectric Newsletter, NOVOCONTROL GmbH, Hundsangen, November 2000.
[5] V. Vogel, Z. Phys., vol. 22, pp. 645, 1921.
[6] G. S. Fulcher, J. Am. Ceram. Soc., vol. 8, pp. 339, 1925.
[7] G. Tammann and W. Z. Hesse, Anorg. Allgem. Chem., vol. 156, pp. 245, 1926.
[8] S. Moreno, and R. Rubio, Macromolecules, vol. 35, pp. 5480, 2002.
[9] G. P. Johari, and M. J. Goldstein, J. Chem. Phys., vol. 53, pp. 2372, 1980.
[10] G. P. Johari, J. Chem. Phys., vol. 28, pp. 1766, 1973.
[11] G. P. Johari, J. Chem. Phys., vol. 28, pp. 1766, 1973.
[12] X. Zhang, and N. Bowler, Dielectric Spectroscopy for Investigation of Plasticization and Reinforcement in Boron Cage Compounds August 31, 2011.
[13] G. Polizos, E. Tuncer, A.L. Agapov, D. Stevens, A.P. Sokolov, M.K. Kidder, J.D. Jacobs, H. Koerner, R.A. Vaia, K.L. More, I. Sauers, Polymer, vol. 53, pp. 595, 2012.